A comprehensive shape factor analysis using transportation of $MoS_2 - SiO_2/H_2O$ inside an isothermal semi vertical inverted cone with porous boundary

E.N. Maraj, Z. Iqbal, Ehtsham Azhar *, Zaffar Mehmood

Department of Mathematics, Faculty of Sciences, HITEC University, Taxila, Pakistan

A B S T R A C T

Background and objectives: Current article gives a comprehensive shape factor analysis of $MoS_2 - SiO_2$ water based hybrid nanofluid in a semi vertical inverted porous cone along with the influence of transverse magnetic field, viscous dissipation and thermal radiation.
Significances: Mathematical investigation is carried out in Cartesian coordinates. Physical flow problem has been tackled numerically by means of shooting algorithm. Effect of significant emerging parameters is displayed and examined through graphs and tables.
Conclusions: It is concluded that the presence of magnetic field resist the fluid flow and boundary layer thickness decreases. Fluid decelerates with an increase in λ and this decrease in fluid flow is more in case of nanofluid when compared with hybrid nanofluid. Velocity decreases with an increase in $S(>0)$. Moreover, it is noticed that the fluid flow decelerates more for SiO_2/water nanofluid as compare to hybrid nanofluid. For both types of nanofluids temperature distribution upsurges with an increase in Eckert number Ec, volumetric fractions ϕ_1 and ϕ_2 in case of nanofluid and hybrid nanofluid, N as well as λ. Moreover, it is evident that the rise of temperature is significantly more for SiO_2/water nanofluid. Furthermore, maximum temperature is achieved for blade shaped nanoparticles suspended in SiO_2/water nanofluid whereas, lowest temperature measurements are observed in case of brick shaped nanoparticles suspended in $MoS_2 - SiO_2$/water hybrid nanofluid. Skin friction coefficient and Nusselt number increases with an increase in nanoparticles volumetric fractions ϕ_1 and ϕ_2 for nano as well as hybrid nanofluid, respectively. Moreover, skin friction coefficient and Nusselt number are of maximum magnitude in case of hybrid nanofluid having blade shaped nanoparticles and minimum magnitude is witnessed for brick shaped nano particles suspended in nanofluid.

© 2018 The Authors. Published by Elsevier B.V. This is an open access article under the CC BY-NC-ND license (http://creativecommons.org/licenses/by-nc-nd/4.0/).

Introduction

In recent years, the problem of two dimensional axisymmetric fluid flows inside a semi vertical inverted cone has been of great interest for many researchers and engineering. Such flows have their significance in numerous engineering and industrial procedures like it plays a vital role in manufacturing industries for the design of reliable equipment for nuclear power plants, gas turbines and several impetus devices for aircraft, missiles, satellites and space vehicles etc. Migration of moisture through air contained in fibrous insulations, grain storage, nuclear waste disposal, dispersion of chemical pollutants through water-saturated soil, and others. Na and Chiou [1] studied the laminar natural convection over a cone frustum. They considered the cases of constant wall temperature and constant wall heat flux and concluded that temperature reduces with an increase in Prandtl number and along the cone surface. Heat and mass transfer by free convection over a truncated cone in a porous medium having variable wall temperature/concentration or variable wall temperature/concentration flux was analyzed by Yih [2]. His work was extended by Chamka [3] in which he considered the effect of magnetic field and thermal radiation. His findings included that all of the local skin-friction coefficients, local Nusselt number, and the local Sherwood number reduced as the magnetic Hartmann number was increased. Some recent articles addressing natural convection phenomenon include [4–6]. Also, while all of these physical parameters decreased with the distance along the cone surface in the presence of the magnetic field, they increased with it in the absence of the magnetic field. In another article magneto hydrodynamic flow has been a subject of

* Corresponding author.
  E-mail address: ehtsham@uaar.edu.pk (E. Azhar).

intense research due to its over whelming importance in numerous fields ranging from several natural phenomena like meteorology, solar physics, cosmic fluid dynamics, astrophysics, geophysics and in the motion of earth's core. The velocity fluctuations are suppressed due to the damping nature of the external magnetic field. This causes a reduction in the turbulent intensity of the MHD flow thereby significantly affecting the thermo fluidic transport. In applications like nuclear fusion reactors, the liquid metal blankets are prone to such magnetic damping phenomena and there is a chance for the degradation of the heat transfer. Some recent articles discussing the influence of magnetic force are cited in Refs. [7–12]. Chamkha and Quadri [13] examined the effect of heat generation/absorption on hydromagnetic flow over a cone embedded in a non-Darcian porous medium. Numerical investigation for micropolar Casson fluid under the influence of internal heating was performed by Mehmood et al. [14]. Recently, Ahmed et al. [15] studied combined effects of internal heat generation and mass transfer taking into the account convective boundary conditions. Influence of thermal radiation and transverse magnetic field on a free convective flow past a vertical isothermal cone surface with chemical reaction was investigated by Afify [16]. Kabeir et al. [17,18] studied micropolar fluid free convection flow over a cone with uniform suction/injection and heat generation/absorption. Noghrehabadi et al. [19] analyzed natural convection flow of a nanofluid over a vertical cone suspended in a non-Darcy porous medium. Some useful contributions are cited in Ref. [20–23] for the reader's interest.

In industry the quality of the final product highly depends on the rate of heat transfer and material thermal conductivity. Most of the fluids encountered in manufacturing industry are of low thermal conductivity. Nano particles suspended in the base fluids, termed as nanofluids are used to overcome this deficiency. Choi and Eastman [24] introduced the pioneer concept of these intelligently engineered fluids. Because of the unique characteristics of nanofluids, they have applications in engineering and medical sciences such as mechanical cooling, heat exchanger, targeted drug delivery, extraction of geothermal forces etc.

Moreover, effect of nanoparticles on natural convective boundary layer flow past a vertical sheet was examined by Kuznetsov and Nield [25]. Later on, Nield and Kuznetsov [26] discussed same problem in porous medium. A considerable amount of research in composition of nanoparticles dispersed in base fluid has risen exponentially. Very recently, Natural convection of nanofluid over vertical plate embedded in porous medium: prescribed surface heat flux was discussed by Noghrehabadi et al. [27]. Zeeshan et al. [28] considered MHD flow of water/ethylene glycol based nanofluid flow with natural convection towards a vertical cone embedded in a porous medium. This work was further extended

by Ellahi et al. [29] in which they studied the shape effects of nano size particles along with entropy generation. Some recent relevant attempts are cited in Refs. [30–36].

Keeping in view the above mentioned attempts present article is a numerical investigation on water based hybrid nanofluid flow towards an inverted porous vertical cone in presence of applied magnetic field and thermal radiation. Moreover, viscous dissipative effects are also taken into the account. Molybdenum disulfide has a layered structure and it is used as a lubricant and catalyst because of its unique properties such as anisotropy, chemically inertness, and photocorrosion resistance. Moreover, MoS_2 nanoparticles product may be used as hydrogenation nanocatalysts. To the best of author's knowledge no attempt has been carried out to examine the viscous dissipative effects on hybrid nanofluid flow towards a porous vertical inverted cone. The physical flow problem has been modeled in Cartesian coordinates and governing coupled nonlinear equations are tackled numerically by means of after simplification. Influence of significant parameters are examined and displayed through graphs and tables. The novel results presented in this article may be useful in academic research and theoretical investigation in designing reliable equipment for nuclear power plants, gas turbines and several impetus devices for aircraft, missiles, satellites and space vehicles etc.

Shape factors and thermal properties of base fluid

This mixture of hybrid nanofluid containing nanoparticles SiO_2 (ϕ_1) and $MoS_2(\phi_2)$ in water taken as base fluid. Moreover the solid volume fraction of SiO_2 has been fixed to 1%. However, the solid volume fraction of MoS_2 varies from 1% to 5%. According to Xie et al. [30] hybrid nanofluid volume fraction is taken as:

$$\phi_{hnf} = \frac{V_{MoS_2} + V_{SiO_2}}{V_{total}} = \phi_1 + \phi_2.$$

In addition, the thermal properties of base fluid and nanoparticles are expressed in Tables 1 and 2 illustrates the effective property of SiO_2/water based nanofluid and MoS_2/SiO_2 hybrid nanofluid.

Table 1
Experimental values of density, specific heat and thermal conductivity for base fluids and nanoparticles (Xie et al. [30] and Iqbal et al. [36]).

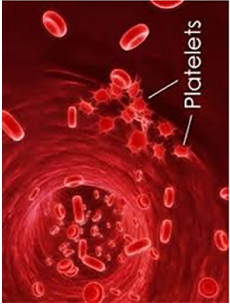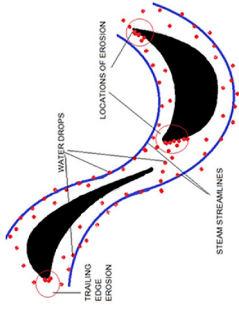| Properties\constituents	Water	SiO_2	MoS_2
Density, ρ (kg/m³)	997	2650	5060
Specific heat, C_p (J/kg K)	4179	730	397.746
Thermal conductivity, k (W/m K)	0.613	1.5	34.5

Table 2
According to Xie et al. [30] and Iqbal et al. [36], expression for Thermophysical charactertistics for nanofluid and hybrid nanofluid.

Properties	Nanofluid	Hybrid Nanofluid
Density	$\rho_{nf} = \rho_f\left[(1-\phi) + \phi\left(\frac{\rho_s}{\rho_f}\right)\right]$	$\rho_{hnf} = \rho_f(1-\phi_2)\left[(1-\phi_1) + \phi_1\left(\rho_{s_1}/\rho_f\right)\right] + \phi_2\rho_{s_2}$
Heat Capacity	$(\rho c_p)_{nf} = (\rho c_p)_f\left[1 - \phi + \phi\frac{(\rho c_p)_s}{(\rho c_p)_f}\right]$	$(\rho c_p)_{hnf} = (\rho c_p)_f(1-\phi_2)\left[(1-\phi_1) + \phi_1\left((\rho c_p)_{s_1}/(\rho c_p)_f\right)\right] + \phi_2(\rho c_p)_{s_2}$
Viscosity	$\mu_{nf} = \frac{\mu_f}{(1-\phi)^{2.5}}$	$\mu_{hnf} = \frac{\mu_f}{(1-\phi_1)^{2.5}(1-\phi_2)^{2.5}}$
Thermal Conductivity	$\frac{k_{nf}}{k_f} = \frac{k_s + (m-1)k_f - (m-1)\phi(k_f - k_s)}{k_s + (m-1)k_f + \phi(k_f - k_s)}$	$\frac{k_{hnf}}{k_f} = \frac{k_{s_2} + (m-1)k_{bf} - (m-1)\phi_2(k_{bf} - k_{s_2})}{k_{s_2} + (m-1)k_{bf} + \phi_2(k_{bf} - k_{s_2})}$ where $\frac{k_{bf}}{k_f} = \frac{k_{s_1} + (m-1)k_f - (m-1)\phi_1(k_f - k_{s_1})}{k_{s_1} + (m-1)k_f + \phi_1(k_f - k_{s_1})}$

where m is shape factor and $\rho_f, \rho_{s_1}, \rho_{s_2}, (c_p)_{hnf}, (c_p)_f, (c_p)_{s_1}, (c_p)_{s_2}$ represents density of fluid, solid nanoparticles of SiO_2, solid nanoparticles of MoS_2, specific heat of hybrid nanofluid, base fluid, solid nanoparticles of SiO_2 and solid nanoparticles of MoS_2, respectively. k_{hnf} is thermal conductivity of hybrid nanofluid, k_f, k_{s_1}, k_{s_2} are thermal conductivity of base fluid, solid nanoparticles of SiO_2 and solid nanoparticles of MoS_2. Table 3 demonstrates the nanoparticles shapes corresponding to distinct values of shape factor.

Table 3
Geometrical appearance of nanoscale particles with their size and sphericity.

Geometrical Appearance				

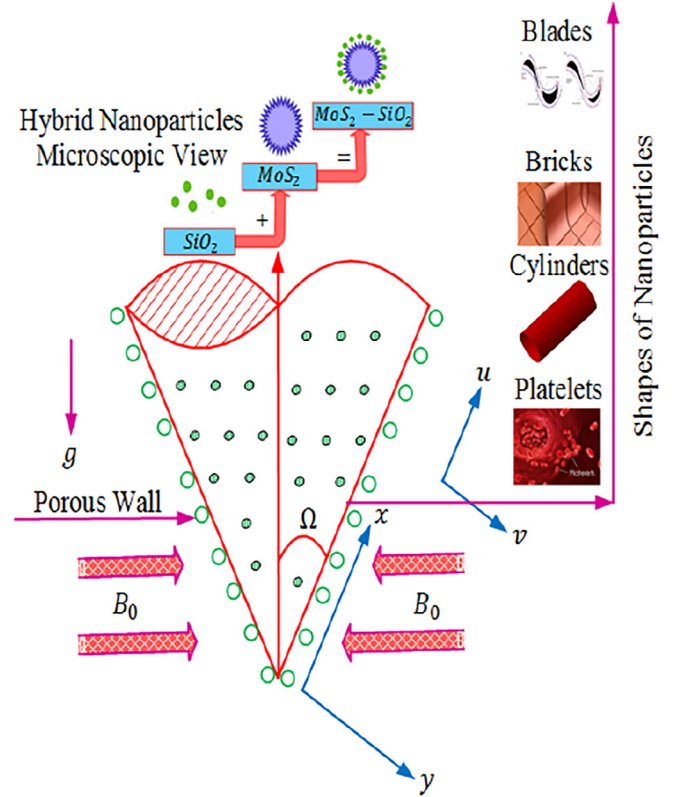| Shape of nanoparticles	Bricks	Cylinders	Platelets	Blades
Size	3.7	4.9	5.7	8.6

Fig. 1. Physical flow diagram.

Problem demonstration in Cartesian Coordinates

This physical problem development contains an inverted iso-thrmal cone with semi vertical angle Ω in which two dimensional, incompressible and steady-state flow of a nanofluid is consider. Further, we take origin of the coordinate system at the vertex of the inverted cone with x-axis is chosen parallel and y-axis taken as normal to the surface of cone. Moreover, heat transfer is incorporated at the surface of an inverted cone in the presence of viscous dissipation and thermal radiation effects. Furthermore, we assumed that temperature T take constant value $T_w = T_\infty + ax^\lambda$ at the wall in which constant $a > 0$, λ is power law index and T_∞ is ambient value of temperature having property $T_w > T_\infty$. This physical background of present engineering problem is explained in Fig. 1.

Under these considerations along with boundary layer approximations, the governing equations are

$$\frac{\partial}{\partial x}(ru) + \frac{\partial}{\partial y}(rv) = 0, \tag{1}$$

$$u\frac{\partial u}{\partial x} + v\frac{\partial u}{\partial y} = \frac{\mu_{hnf}}{\rho_{hnf}}\left(\frac{\partial^2 u}{\partial y^2}\right) + \frac{(\rho\beta)_{hnf}}{\rho_{hnf}}g(T - T_\infty) - \frac{\sigma^2\beta^2 u}{\rho_{hnf}}, \tag{2}$$

$$u\frac{\partial T}{\partial x} + v\frac{\partial T}{\partial y} = \alpha_{hnf}\frac{\partial^2 T}{\partial y^2} + \frac{\mu_{hnf}}{(\rho c_p)_{hnf}}\left(\frac{\partial u}{\partial y}\right)^2 - \frac{1}{(\rho c_p)_{hnf}}\frac{\partial q_r}{\partial y}, \tag{3}$$

with associated boundary conditions are

$$u(x,0) = 0, \quad v(x,0) = v_w, \quad u(x,\infty) \to 0,$$
$$T(x,0) = T_w = T_\infty + ax^\lambda, \quad T(x,\infty) \to T_\infty, \tag{4}$$

in which u and v are velocity components in x- and y-directions respectively with thin boundary layer $r = x\sin\Omega$. Moreover, ρ_{hnf} is hybrid nanofluid density, μ_{hnf} is dynamic viscosity of hybrid nanofluid, σ is electrical conductivity, T is temperature, q_r radiative heat flux, g is gravitational acceleration and v_w is suction/injunction

velocity at the surface of an inclined vertical cone, respectively. Moreover in view of Rosseland approximation the radiative heat flux is given by

$$q_r = -\frac{4\sigma^*}{3k^*}\frac{\partial T^4}{\partial r}, \tag{5}$$

in which σ^* is Stefan–Boltzmann constant and k^* is mean proportion coefficient. Under the assumption of temperature diffusion within the flow are sufficiently small, we may expand the term T^4 as a linear function of temperature in Taylor series about T_∞ and neglecting the higher terms, one can get

$$T^4 \approx 4T_\infty^3 T - 3T_\infty^4. \tag{6}$$

To further facilitate the present analysis we consider stream function $\psi(x,y)$ as

$$u = \frac{1}{r}\frac{\partial \psi}{\partial y}, \quad v = -\frac{1}{r}\frac{\partial \psi}{\partial x}, \tag{7}$$

where $\psi = v_f r G_{r_x}^{\frac{1}{4}} f(\eta)$ in which G_{r_x} is known as Rayleigh number and mathematically can be expressed as

$$G_{r_x} = \frac{(\rho\beta)_{hnf} g \cos\Omega (T_w - T_\infty) x^3}{v_f^2}. \tag{8}$$

In view of Eqs. (7) and (8), we introduce following similarity transformation

$$u = \frac{v_f}{x} G_{r_x}^{\frac{1}{2}} f', \quad v = -\frac{v_f}{x} G_{r_x}^{\frac{1}{4}}(\eta f' - f), \quad \eta = \frac{x}{y} G_{r_x}^{\frac{1}{4}}, \quad \theta(\eta) = \frac{T - T_\infty}{T_w - T_\infty}, \tag{9}$$

Eq. (1) is automatically satisfied and Eqs. (2) and (3) along with boundary conditions (4) associated with Rosseland approximation for radiative heat flux (5), are reduced to the following nonlinear set of differential equations

$$\left(\frac{\lambda+1}{4}\right)(f')^2 - \left(\frac{\lambda+7}{4}\right)ff'' = \frac{1}{\Phi_1}f''' - \frac{M^2 f'}{\Phi_2} + \theta, \tag{10}$$

$$\Pr\left[\lambda\theta f' - \left(\frac{\lambda+7}{4}\right)f\theta' - Ec(f'')^2\right] = \frac{1}{\Phi_3}\frac{k_{hnf}}{k_f}(1+N)\theta'', \tag{11}$$

$$\left.\begin{array}{l} f = S, f' = 0, \theta = 1 \quad \text{when } \eta = 0 \\ f' \to 0, \theta \to 0, \qquad \text{when } \eta \to \infty \end{array}\right\}. \tag{12}$$

in which

$$\Phi_1 = (1-\phi_1)^{2.5}(1-\phi_2)^{2.5}[(1-\phi_2)\{(1-\phi_1)$$
$$+\phi_1\left(\rho_{s_1}/\rho_f\right)\} + \phi_2\rho_{s_2}/\rho_f], \tag{13}$$

$$\Phi_2 = (1-\phi_2)\left[(1-\phi_1) + \phi_1\left(\rho_{s_1}/\rho_f\right)\right] + \phi_2\rho_{s_2}/\rho_f, \tag{14}$$

$$\Phi_3 = (1-\phi_2)\left[(1-\phi_1) + \phi_1\left((\rho c_p)_{s_1}/(\rho c_p)_f\right)\right] + \phi_2(\rho c_p)_{s_2}/(\rho c_p)_f. \tag{15}$$

Where $f(0) = S$ with $S < 0$ corresponds to suction case and $S > 0$ implies injection. Moreover, in above expression dimensionless quantities such as Prandtl number Pr, Eckert number Ec, Hartman number M, and radiation parameter N are defined as

$$\Pr = \frac{\mu_f(c_p)_f}{k_f}, \quad Ec = \frac{\mu_f x^2}{G_{r_x}^{\frac{1}{2}}}, \quad M = \frac{\sigma_{hnf} B_0^2 x^2}{\mu_f G_{r_x}^{\frac{1}{2}}},$$

$$N = \frac{16T_\infty^3 x^2}{3k^* k G_{r_x}^{\frac{1}{2}} \mu_f(c_p)_f}, \quad S = \frac{v_w x}{v_f G_{r_x}^{\frac{1}{4}}}. \tag{16}$$

The physical quantities of interest are skin friction coefficient C_f and local Nusselt number Nu_x, which are defined as

$$C_f = \frac{\tau_{xy}}{\rho_{hnf} u_w^2}, \quad Nu_x = \frac{q_w}{k_{hnf}(T_w - T_\infty)}, \tag{17}$$

where the wall friction τ_{xy} and heat transfer q_w are defined as

$$\left\{\begin{array}{l} \tau_{xy} = \mu_{hnf}\left(\frac{\partial u}{\partial y}\right)\Big|_{y=0}, \\ q_w = -k_{hnf}\left(\frac{\partial T}{\partial y}\right) + (q_r)_w\Big|_{y=0}. \end{array}\right\} \tag{18}$$

In view of (8), expressions described in (13), provided the following dimensionless skin friction $C_f G_{r_x}^{\frac{1}{4}}$ and local Nusselt Nu_x as

$$C_f G_{r_x}^{\frac{1}{4}} = \frac{1}{(1-\phi)^{2.5}} f''(0),$$

$$Nu_x = -\left(\frac{k_{hnf}}{k_f} + N\right)\theta'(0). \tag{19}$$

Computational procedure

The coupled non-linear governing boundary layer Eqs. (9) and (10) together with boundary conditions (11) are solved numerically by using Runge–Kutta fifth order technique along with shooting method. Firstly higher order non-linear differential Eqs. (9) and (10) are converted into system of first order differential equations and further transformed into initial value problem by labeling the variables as $(f, f', f'', \theta, \theta')^T = (y_1, y_1' = y_2, y_2' = y_3, y_4, y_4' = y_5)^T$. According to the numerical procedure the above system of equations are formulated as

$$\begin{pmatrix} y_1' \\ y_2' \\ y_3' \\ y_4' \\ y_5' \end{pmatrix} = \begin{pmatrix} y_2 \\ y_3 \\ \Phi_1\left(\left(\frac{\lambda+1}{4}\right)(y_2)^2 - \left(\frac{\lambda+7}{4}\right)y_1 y_3 + \frac{M^2}{\Phi_2}y_2 - y_4\right) \\ y_5 \\ \frac{\Pr}{(1/\Phi_3)\left(k_{hnf}/k_f\right)(1+N)}\left(\lambda y_2 y_4 - \left(\frac{\lambda+7}{4}\right)y_1 y_5 - Ec(y_3)^2\right) \end{pmatrix}, \tag{20}$$

Table 4
Effect of Nanoparticles fractions on skinfriction and Nusselt number for MoS_2/water and $MoS_2 - SiO_2$/water when $M = 0.4, \lambda = 1.0, S = 0.1, Ec = 0.5, N = 0.4$.

	ϕ_1/ϕ_2	$m = 3.7$		$m = 4.9$		$m = 5.7$		$m = 8.6$	
		Nano	Hybrid	Nano	Hybrid	Nano	Hybrid	Nano	Hybrid
	0.04	0.9315	1.2788	0.9325	1.2970	0.9330	1.3079	0.9340	1.3420
C_f	0.08	1.0236	1.5056	1.0256	1.5355	1.0265	1.5557	1.0286	1.6175
	0.12	1.1224	1.7423	1.1254	1.7922	1.1268	1.8215	1.1299	1.9091
	0.04	1.5165	1.5963	1.5183	1.6278	1.5192	1.6473	1.5211	1.7109
Nu	0.08	1.5174	1.6766	1.5209	1.7354	1.5225	1.7720	1.5263	1.8919
	0.12	1.5178	1.7585	1.5219	1.8442	1.5243	1.8977	1.5297	2.0717

Table 5
Effect of suction parameter S on skinfriction and Nusselt number for MoS_2/water and $MoS_2 - SiO_2$/water when $M = 0.4, \lambda = 1.0, \phi_1 = \phi_2 = 0.1, Ec = 0.5, N = 5.0$.

		m = 3.7		m = 4.9		m = 5.7		m = 8.6	
	S	Nano	Hybrid	Nano	Hybrid	Nano	Hybrid	Nano	Hybrid
C_f	0.1	1.6033	2.3204	1.6056	2.3602	1.6067	2.3838	1.6093	2.4546
	0.2	1.5806	2.3337	1.5835	2.3824	1.5849	2.4111	1.5880	2.4972
	0.3	1.5428	2.3385	1.5463	2.3866	1.5480	2.4208	1.5517	2.5233
Nu	0.1	0.7446	0.8838	0.7474	0.9288	0.7487	0.9568	0.7517	1.0469
	0.2	0.8722	1.0004	0.8749	1.0445	0.8762	1.0718	0.8791	1.1603
	0.3	1.0121	1.1259	1.0147	1.1685	1.0159	1.1950	1.0186	1.2810

Table 6
Effect of Eckert number Ec on skinfriction and Nusselt number for MoS_2/water and $MoS_2 - SiO_2$/water when $M = 0.4, \lambda = 1.0, S = 0.1, \phi_1 = \phi_2 = 0.1, N = 5.0$.

		m = 3.7		m = 4.9		m = 5.7		m = 8.6	
	Ec	Nano	Hybrid	Nano	Hybrid	Nano	Hybrid	Nano	Hybrid
C_f	0.5	1.6033	2.3204	1.6056	2.3602	1.6067	2.3838	1.6093	2.4546
	1.0	1.6178	2.3401	1.6202	2.3798	1.6213	2.4032	1.6238	2.4735
	1.5	1.6329	2.3606	1.6352	2.3999	1.6363	2.4232	1.6388	2.4930
Nu	0.5	0.7446	0.8838	0.7474	0.9288	0.7487	0.9568	0.7517	1.0469
	1.0	0.6961	0.8228	0.6987	0.8670	0.6999	0.8908	0.7027	0.9750
	1.5	0.6454	0.7592	0.6478	0.7981	0.6490	0.8222	0.6515	0.9006

Table 7
Effect of thermal radiation parameter N on skinfriction and Nusselt number for MoS_2/water and $MoS_2 - SiO_2$/water when $M = 0.4, \lambda = 0.1, S = 0.1, \phi_1 = \phi_2 = 0.1$, $Ec = 3.0$.

		m = 3.7		m = 4.9		m = 5.7		m = 8.6	
	N	Nano	Hybrid	Nano	Hybrid	Nano	Hybrid	Nano	Hybrid
C_f	0.1	1.1781	1.8238	1.1813	1.8766	1.1828	1.9076	1.1862	2.0005
	0.2	1.2198	1.8777	1.2229	1.9300	1.2244	1.9607	1.2277	2.0525
	0.3	1.2578	1.9269	1.2609	1.9785	1.2624	2.0089	1.2657	2.0998
Nu	0.1	0.9347	0.8086	0.9341	0.7997	0.9338	0.7949	0.9331	0.7827
	0.2	0.8491	0.9329	0.8485	0.7256	0.8482	0.7218	0.8476	0.7130
	0.3	0.7775	0.6702	0.7770	0.6644	0.7768	0.6615	0.7763	0.6557

Table 8
Comparison for values of skin friction coefficient with Awad et al. [37] when $\phi_1 = \phi_2 = 0.0$.

	Awad et al. [37]		Present Results
λ	BVP4c	RK6	
0.0	1.0857945	1.0857945	1.0857945
0.3	1.0457628	1.0457628	1.0457628
0.6	1.0122259	1.0122259	1.0122259
1.0	0.9748621	0.9748621	0.9748621

Table 9
Comparison for values of Nusselt number with Awad et al. [37] when $\phi_1 = \phi_2 = 0.0$ and $N = 0$.

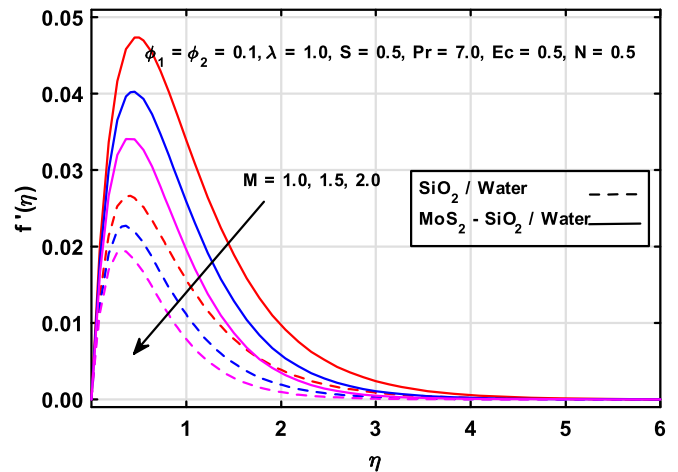|	Awad et al. [37]		Present Results
λ	BVP4c	RK6	
0.0	0.5063661	0.5063661	0.5063661
0.3	0.5524177	0.5524177	0.5524177
0.6	0.5915881	0.5915881	0.5915881
1.0	0.6361635	0.6361635	0.6361635

Fig. 2. Variation of M on $f'(\eta)$.

$$\begin{pmatrix} y_1(0) \\ y_2(0) \\ y_3(0) \\ y_4(0) \\ y_5(0) \end{pmatrix} = \begin{pmatrix} S \\ 0 \\ S_1 \\ 1 \\ S_2 \end{pmatrix}. \qquad (21)$$

Appropriate values of unknown initial conditions S_1 and S_2 are approximated through Newton's method. Computations are carried out using mathematics software MATLAB. End of boundary layer region i.e.,when $\eta \to \infty$ to each group of parameters, is determined when the values of unknown boundary conditions do not change to a successful loop with error less than 10^{-6}.
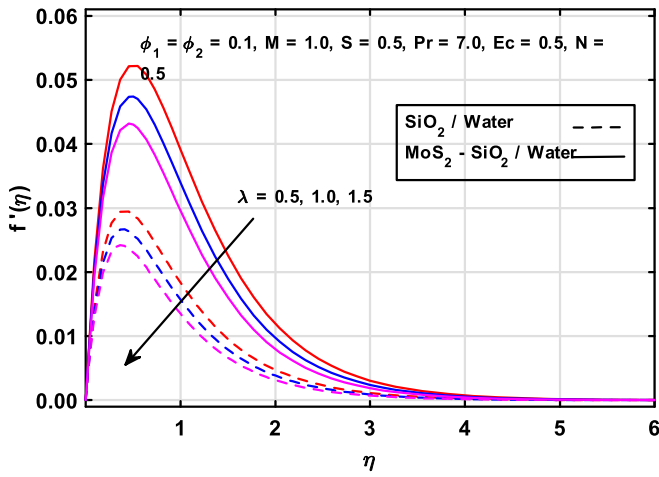
Fig. 3. Variation of λ on $f'(\eta)$.
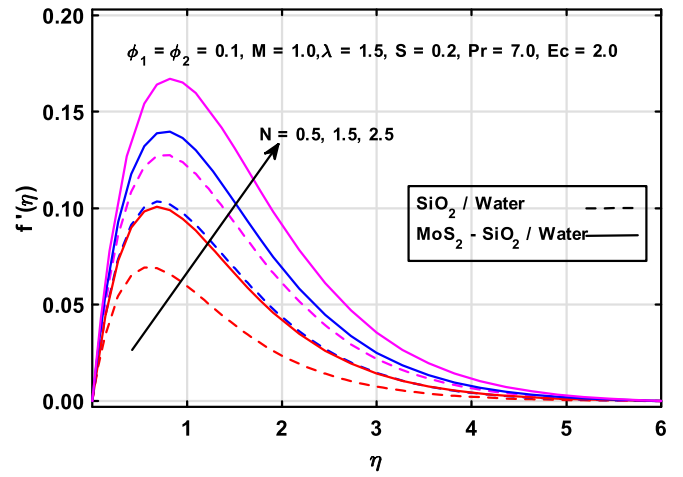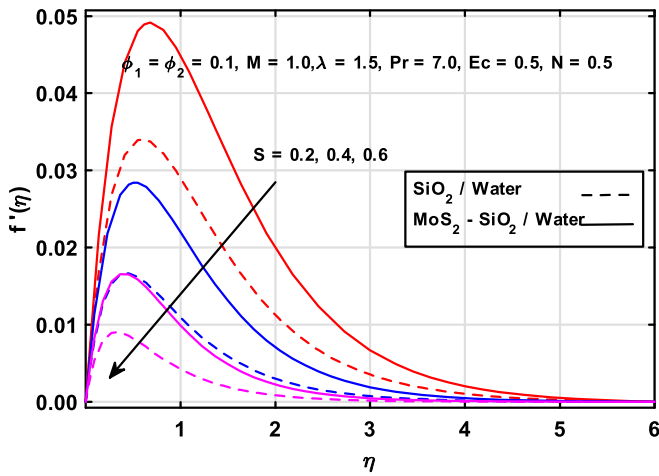

Fig. 6. Variation of N on $f'(\eta)$.

Fig. 4. Variation of S on $f'(\eta)$.
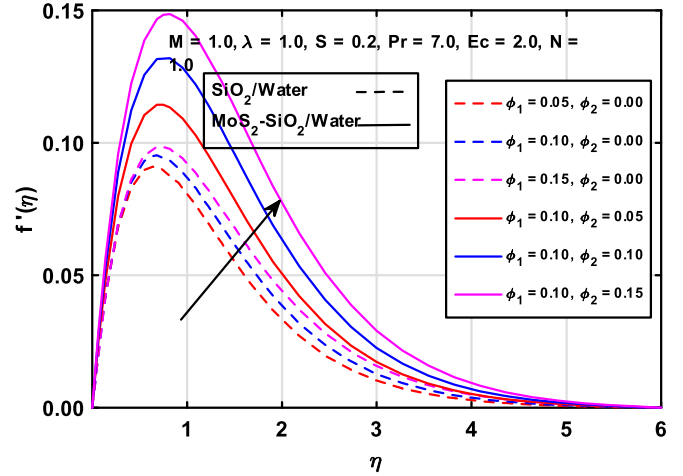

Fig. 7. Variation of ϕ_1 and ϕ_2 on $f'(\eta)$.
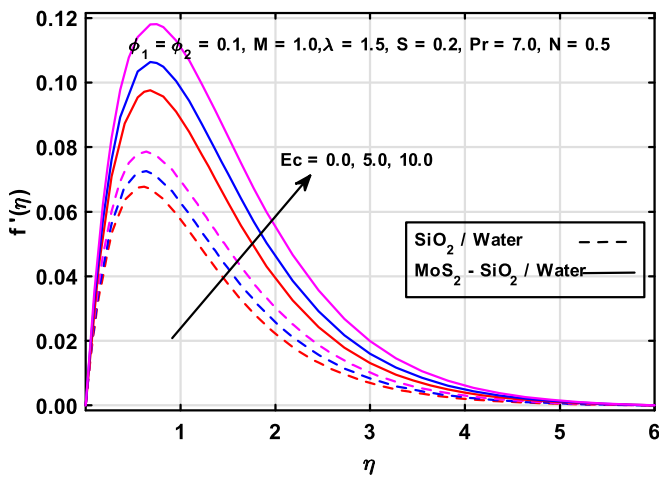

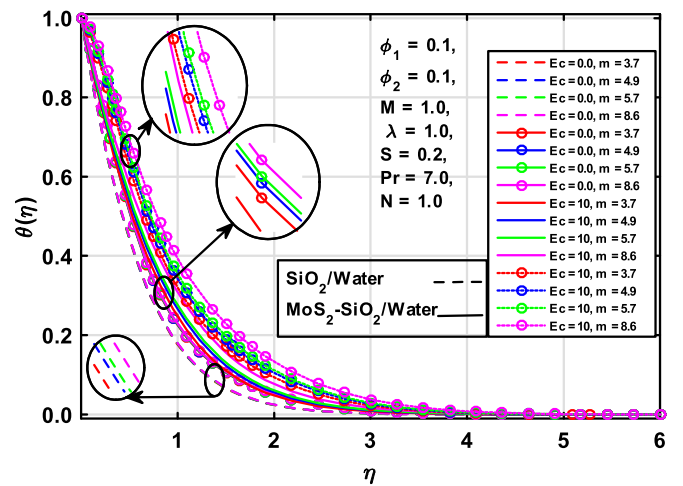**Fig. 5.** Variation of Ec on $f'(\eta)$.

Fig. 8. Variation of Ec on $\theta(\eta)$.

Theoretical results description

In this section the computational results of fluid velocity and temperature distributions carried out in previous section are examined for the effects of prominent physical parameters by means of graphical presentations. Moreover, tables are drawn for meaningful physical quantities namely, coefficient of skin friction and Nusselt number for different nanoparticles shape factors in
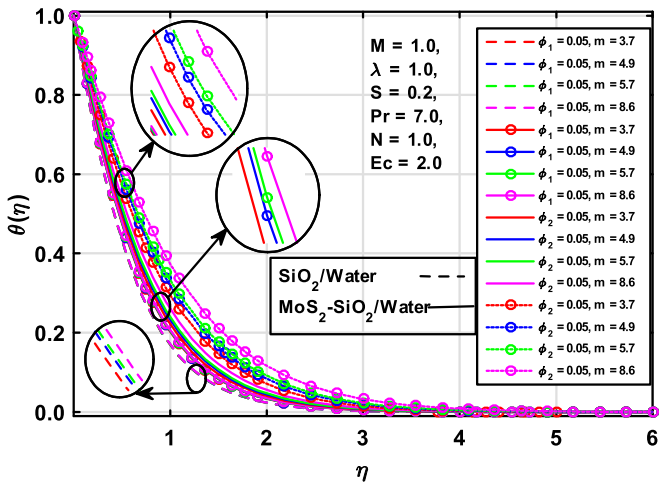
Fig. 9. Variation of ϕ_1 and ϕ_2 on $\theta(\eta)$.
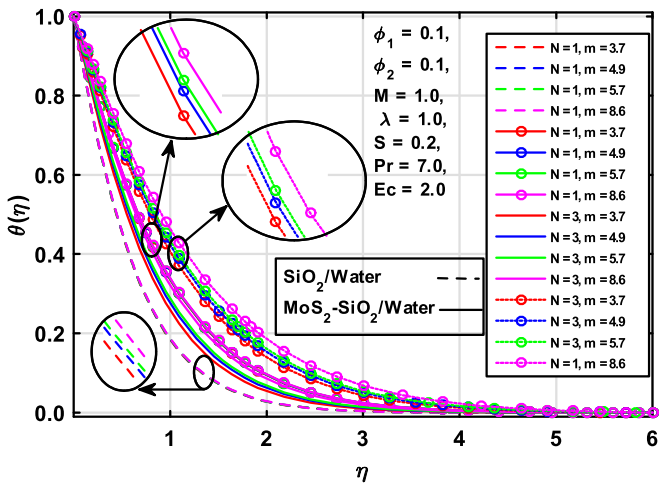

Fig. 10. Variation of N on $\theta(\eta)$.

Fig. 11. Variation of λ on $\theta(\eta)$.

Fig. 12. Streamlines for $\lambda = 1$.

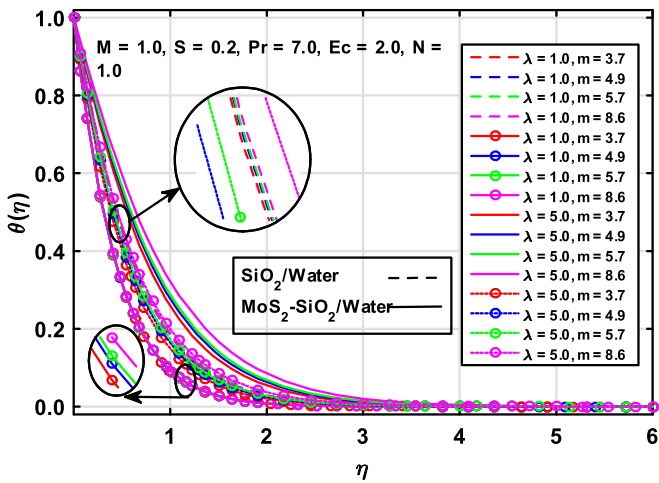**Fig. 13.** Streamlines for $M = 2$.

case of nanofluid and hybrid nanofluid, respectively. In this regard, Figs. 2–7 are plotted to study the influence of significant emerging parameters on SiO_2/water nanofluid and $MoS_2 - SiO_2$/water hybrid nanofluid velocity distri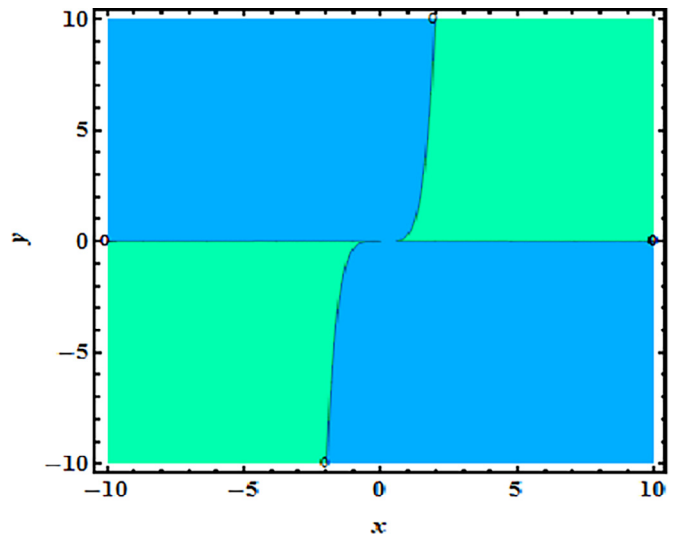butions. In these figures sol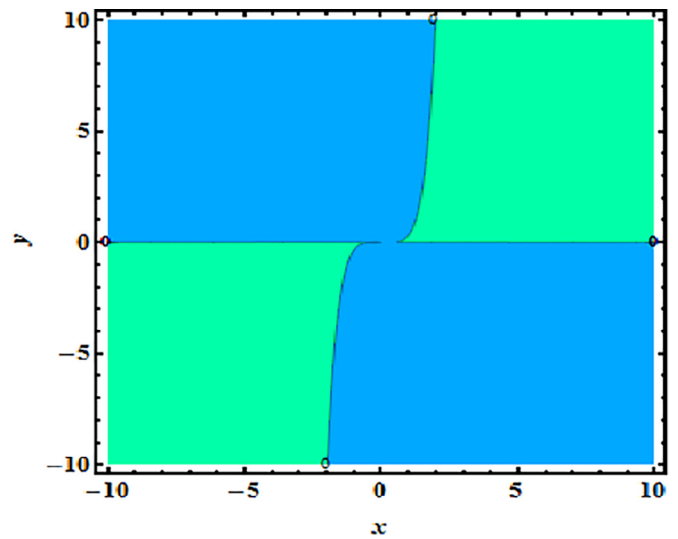id lines depict the behavior of $MoS_2 - SiO_2$/water hybrid nanofluid and dashed lines are used to display the results for SiO_2/water nanofluid, respectively. Fig. 2 displays the effect of magnetic parameter M on fluid flow and from this figure it is evident that presence of magnetic field resist the fluid flow for both types of nanofluids and viscous boundary layer thickness decreases. Moreover, it is noticed that the fluid flow decelerates more for SiO_2/water nanofluid as compare to hybrid nanofluid. Influence of power law index λ is examined through Fig. 3. It is depicted that fluid decelerates with an increase in λ and this decrease in fluid flow is more in case of nanofluid when compared with hybrid nanofluid. From this figure it is concluded that the power law of temperature prescribed on the frustum leads to decelerates fluid flow. Fig. 4 shows the effect of suction parameter on both types of nanofluid flow. From this figure it is evident that the velocity decreases with an increase in $S(> 0)$ due to the fact that the suction at the surface acts in an opposing manner leading to decelerate fluid flow. Moreover, decrease in velocity of nanofluid is significantly more than hybrid nanofluid. Influence of Eckert number Ec is displayed in Fig. 5. From this figure it is witnessed that the increase in Eckert number contribute in accelerating both types of nanofluid flow. This

happens mainly because Ec is the ratio of advective transport to heat dissipation potential. The increase in Eckert number indicates an increase in advective transport of fluid which is an increase in the fluid velocity and momentum boundary layer thickness. Moreover, this increase is significantly more in case of hybrid nanofluid. Fig. 6 is plotted to examine the effect of thermal radiation on both types of nanofluid velocity. It is observed that the increase in thermal radiation parameter N contributes in accelerating the fluid flow and momentum boundary layer thickness of both nano and hybrid nanofluids. Contribution of nano and hybrid nano volumetric fractions are examined through Fig. 7. It is depicted that fluid velocity upsurges with the increase in nanoparticle volumetric fractions. In case of hybrid nanofluid volumetric fraction of SiO_2 has been kept fixed to 1%. The increase in velocity is due to the fact that dynamic viscosity of both nanofluid and hybrid nanofluid are in reverse relation with nanoparticles volumetric fractions. Thus, the increase in ϕ_1 and ϕ_2 leads to decrease base fluid viscosity and as a consequence fluid flow accelerates. Moreover, from Fig. 7 it is observed that fluid velocity is more in case of hybrid nanofluid.

Figs. 8–11 are plotted to study the influence of meaningful emerging parameters on temperature distribution of nano and hybrid nanofluid. Fig. 8 is plotted for distinct values of Eckert number keeping in mind four distinct values of nanoparticles shape factors for nano as well as hybrid nanofluids. From this figure it is revealed that for both types of nanofluids temperature distribution upsurges with an increase in Eckert number. This happens because Eckert number indicates the viscous dissipative effects and the kinetic energy produced due to resistance of viscous forces in fluid flow leads to rise temperature. Influence of nanoparticles volumetric fractions are displayed in Fig. 9. It is observed that the increase in the volumetric fractions ϕ_1 and ϕ_2 in case of nanofluid and hybrid nanofluid leads to rise temperature, respectively. Figs. 10 and 11 are plotted for rising values of thermal radiation parameter N and power law index λ, respectively. From these figures it is concluded that nanofluid as well as hybrid nanofluid temperature distributions rises with an increase in N as well as λ. Moreover, it is evident that the rise of temperature is significantly more for SiO_2/water nanofluid for rising values of Eckert number, ϕ_1, thermal radiation parameter and power law index. Furthermore, maximum temperature is achieved for blade shaped nanoparticles suspended in SiO_2/water nanofluid whereas, lowest temperature measurements are observed in case of brick shaped nanoparticles suspended in $MoS_2 - SiO_2$/water hybrid nanofluid. Detailed study of these figures reveals that hybrid nanofluids play significant role in fluid transport and higher temperature distribution is achieved for nanofluid. Figs. 12 and 13 shows the flow pattren for distinct values of λ and magnetic parameter.

Tables 4–7 are listed to examine the effect of nanoparticles volumetric fractions ϕ_1 and ϕ_2, suction parameter S, Eckert number Ec and N on skin friction coefficient and Nusselt number for nano and hybrid nanofluid corresponding to distinct shape factor of nanoparticles,respectively. From these tables it is revealed that both skin friction coefficient and Nusselt number increases with an increase in nanoparticles volumetric fractions ϕ_1 and ϕ_2 for nano as well as hybrid nanofluid, respectively. Moreover, skin friction coefficient and Nusselt number are of maximum magnitude in case of hybrid nanofluid having blade shaped nanoparticles and minimum magnitude is witnessed for brick shaped nano particles suspended in nanofluid. Skin friction coefficient rises with an increase in suction parameter S in case of SiO_2/water nanofluid while opposite trend is witness for $MoS_2 - SiO_2$/water hybrid nanofluid. Minimum magnitude is witness for brick shaped nanoparticles suspended in SiO_2/water nanofluid and maximum magnitude is observed for blade shaped nanoparticles suspended in

$MoS_2 - SiO_2$/water hybrid nanofluid see Table 5. Moreover, from Table 5 it is observed that Nusselt number increases for rising values of suction parameter in case of both nano and hybrid nanofluids. Effect of Eckert number Ec is studied through Table 6. It is revealed that skin friction coefficient increases and Nusselt number decreases with an increase in viscous dissipation i.e., Ec and thermal radiation parameter N see Table 7. Tables 8 and 9 are the comparison for values of skin friction coefficient and Nusselt number in a absence of nanoparticles with those of Awad et al. [37]. It is evident that the present results are in good agreement with results available in literature (Figs. 2–13).

Conclusions and novelty of article

Present article was a numerical investigation for convection from an inverted cone having porous surface in case of SiO_2/water nanofluid and $MoS_2 - SiO_2$/water hybrid nanofluidic transport. The investigation was carried out for both types of nanofluid velocity and temperature distributions along with skin friction coefficient and Nusselt number taking into the account for distinct nanoparticles shape factors. The governing system of differential equations were simplified and solved numerically by means of shooting algorithm with the aid of computational software MATLAB. Key findings of present analysis include that the presence of magnetic field resist the fluid flow for both types of nanofluids and viscous boundary layer thickness decreases.

Fluid decelerates with an increase in λ and this decrease in fluid flow is more in case of nanofluid when compared with hybrid nanofluid. Velocity decreases with an increase in $S(>0)$. Moreover, it is noticed that the fluid flow decelerates more for SiO_2/water nanofluid as compare to hybrid nanofluid. The increase in Eckert number contribute in accelerating both types of nanofluid flow. Moreover, this increase is significantly more in case of hybrid nanofluid.

Increase in thermal radiation parameter N contributes in accelerating the fluid flow and momentum boundary layer thickness of both nano and hybrid nanofluids. For both types of nanofluids temperature distribution upsurges with an increase in Eckert number Ec, volumetric fractions ϕ_1 and ϕ_2 in case of nanofluid and hybrid nanofluid, N as well as λ. Moreover, it is evident that the rise of temperature is significantly more for SiO_2/water nanofluid. Furthermore, maximum temperature is achieved for blade shaped nanoparticles suspended in SiO_2/water nanofluid whereas, lowest temperature measurements are observed in case of brick shaped nanoparticles suspended in $MoS_2 - SiO_2$/water hybrid nanofluid. Detailed study of these figures reveals that hybrid nanofluids play significant role in fluid transport and higher temperature distribution is achieved for nanofluid.

Skin friction coefficient and Nusselt number increases with an increase in nanoparticles volumetric fractions ϕ_1 and ϕ_2 for nano as well as hybrid nanofluid, respectively. Moreover, skin friction coefficient and Nusselt number are of maximum magnitude in case of hybrid nanofluid having blade shaped nanoparticles and minimum magnitude is witnessed for brick shaped nano particles suspended in nanofluid. Skin friction coefficient rises with an increase in suction parameter S in case of SiO_2/water nanofluid while opposite trend is witness for $MoS_2 - SiO_2$/water hybrid nanofluid. Minimum magnitude is witness for brick shaped nanoparticles suspended in SiO_2/water nanofluid and maximum magnitude is observed for blade shaped nanoparticles suspended in $MoS_2 - SiO_2$/water hybrid nanofluid. Nusselt number increases for rising values of suction parameter in case of both nano and hybrid nanofluids. Skin friction coefficient increases and Nusselt number decreases with an increase in viscous dissipation and thermal radiation.

References

[1] Na TY, Chiou JP. Laminar natural convection over a frustum of a cone. Appl. Sci. Res. 1979;35:409–21.

[2] Yih KA. Coupled heat and mass transfer by free convection over a truncated cone in porous media: VWT/VWC or VHF/VMF. Acta Mech. 1999;137:83–97.

[3] Chamkha AJ. Coupled heat and mass transfer by natural convection about a truncated cone in the presence of magnetic field and radiation effects. Numer. Heat Transfer Part A: Appl. 2001;39:511–30.

[4] Selimefendigil F, Öztop H, Abu-Hamdeh N. Natural convection and entropy generation in nanofluid filled entrapped trapezoidal cavities under the influence of magnetic field. Entropy 2016;18:43–65.

[5] Selimefendigil F, Öztop H. Natural convection in a flexible sided triangular cavity with internal heat generation under the effect of inclined magnetic field. J. Magn. Magn. Mat. 2016;417:327–37.

[6] Selimefendigil F, Öztop H. Natural convection and entropy generation in nanofluid filled entrapped trapezoidal cavities under the influence of magnetic field. J. Heat Transf. 2017;138:122501.

[7] Iqbal Z, Mehmood R, Mehmood Z. Thermal deposition on magnetohydrodynamic nanofluidic transport of viscoplastic fluid with microrotations. J. Mol. Liq. 2017;243:341–7.

[8] Maraj EN, Akbar NS, Iqbal Z, Azhar E. Framing the MHD mixed convective performance of CNTs in rotating vertical channel inspired by thermal deposition: Closed form solutions. J. Mol. Liq. 2017;233:334–43.

[9] Selimefendigil F, Öztop H. MHD mixed convection and entropy generation of power law fluids in a cavity with a partial heater under the effect of a rotating cylinder. Int. J. Heat Mass Transf. 2016;98:40–51.

[10] Iqbal Z, Akbar NS, Azhar E, Maraj EN. MHD rotating transport of CNTS in a vertical channel submerged with Hall current and oscillations. Eur. Phys. J. Plus. 2017;132:143–57.

[11] Mahmood T, Shahzad A, Iqbal Z, Ahmed J, Khan M. Computational modelling on 2D magnetohydrodynamic flow of Sisko fluid over a time dependent stretching surface. Results Phys. 2017;7:832–42.

[12] Mahmood T, Iqbal Z, Ahmed J, Shahzad A, Khan M. Combined effects of magnetohydrodynamics and radiation on nano Sisko fluid towards a nonlinear stretching sheet. Results Phys. 2017;7:2458–69.

[13] Chamkha AJ, Quadri MMA. Combined heat and mass transfer by hydromagnetic natural convection over a cone embedded in a non-Darcian porous medium with heat generation/absorption effects. Heat Mass Transf. 2002;38:487–95.

[14] Mehmood Z, Mehmood R, Iqbal Z. Numerical Investigation of Micropolar Casson Fluid over a Stretching Sheet with Internal Heating. Commun. Theor. Phys. 2017;67:443–8.

[15] Ahmed B, Iqbal Z, Azhar E. Combined effects of internal heat generation and mass effects on MHD Casson fluid with convective boundary conditions. Int. J. Appl. Electrom. Mech. 2017;1:1–11.

[16] Afify AA. The effect of radiation on free convective flow and mass transfer past a vertical isothermal cone surface with chemical reaction in the presence of a transverse magnetic field. Can. J. Phy. 2004;82:447–58.

[17] El- Kabeir SMM, Modather M, Mansour MA. Effect of heat and mass transfer on free convection flow over a cone with uniform suction or injection in micro polar fluids. Int. J. Appl. Mech. Eng. 2006;11:15–35.

[18] El-Kabeir SMM, Abdou MMM. Chemical reaction, heat and mass transfer on MHD flow over a vertical isothermal cone surface in micropolar fluids with heat generation/absorption. Appl. Math. Sci. J. Theor. Appl. 2007;1:1663–74.

[19] Noghrehabadi A, Behseresht A, Ghalambaz M, Behseresht J. Natural convection flow of nanofluids over a vertical cone embedded in a non-Darcy porous medium. J. Thermophys. Heat Transfer 2013;27:334–41.

[20] Selimefendigil F, Öztop HF. Mixed convection of nanofluids in a three dimensional cavity with two adiabatic inner rotating cylinders. Int. J. Heat Mass Transf. 2017;117:331–43.

[21] Selimefendigil F, Öztop H. Fluid–structure-magnetic field interaction in a nanofluid filled lid-driven cavity with flexible side wall. Eur. J. Mech.-B/Fluids 2017;61:77–85.

[22] Iqbal Z, Ahmed B. Performance of thermal deposition and mass flux condition on bioconvection nanoparticles containing gyrotactic microorganisms. Eur. Phys. J. Plus 2017;132:486–501.

[23] Iqbal Z, Akbar NS, Azhar E, Maraj EN. Performance of hybrid nanofluid (Cu-CuO/water) on MHD rotating transport in oscillating vertical channel inspired by Hall current and thermal radiation. Alexandria Engg. J. 2017. https://doi.org/10.1016/j.aej.2017.03.047.

[24] S.U.S. Choi, J.A. Eastman, Enhancing thermal conductivity of fluids with nanoparticles, in: The Proceedings of the 1995 ASME International Mechanical Engineering Congress and Exposition, ASME, San Francisco, USA, 1995, 99–105. FED 231/MD 66.

[25] Kuznetsov V, Nield DA. Natural convective boundary-layer flow of a nanofluid past a vertical plate. Int. J. Therm. Sci. 2010;49:243–7.

[26] Nield DA, Kuznetsov AV. The Cheng-Minkowycz problem for natural convective boundary-layer flow in a porous medium saturated by a nanofluid. Int. J. Heat Mass Transfer 2009;52:5792–5.

[27] Noghrehabadi A, Behseresht A, Ghalambaz M. Natural convection of nanofluid over vertical plate embedded in porous medium: prescribed surface heat flux. Appl. Math. Mech. 2013;34:669–86.

[28] Zeeshan A, Ellahi R, Hassan M. Magnetohydrodynamic flow of water/ethylene glycol based nanofluids with natural convection through a porous medium. Eur. Phys. J. Plus 2014;129:261–71.

[29] Ellahi R, Hassan M, Zeeshan A. Shape effects of nanosize particles in $Cu - H_2O$ nanofluid on entropy generation. Int. J. Heat Mass Transf. 2015;81:449–56.

[30] Xie H, Jiang B, Liu B, Wang Q, Xu J, Pan F. An investigation on the tribological performances of the $SiO_2 - MoS_2$ hybrid nanofluids for magnesium alloy-steel contacts. Nanoscale Res. Lett. 2016;11:329–36.

[31] Selimefendigil F, Öztop HF. Jet impingement cooling and optimization study for a partly curved isothermal surface with CuO-water nanofluid. Int. Commun. Heat Mass Transf. 2017;89:211–8.

[32] Selimefendigil F, Öztop HF, Hamdeh NA. Mixed convection due to rotating cylinder in an internally heated and flexible walled cavity filled with SiO_2-water nanofluids: Effect of nanoparticle shape. Int. Commun. Heat Mass Transf. 2017;71:9–19.

[33] Selimefendigil F, Öztop HF. Effects of nanoparticle shape on slot-jet impingement cooling of a corrugated surface with nanofluids. J. Therm. Sci. Engg. Appl. 2017;9:021016.

[34] Selimefendigil F, Öztop H. Natural convection and entropy generation in nanofluid filled entrapped trapezoidal cavities under the influence of magnetic field. J. Heat Transf. 2017;138:122501.

[35] Selimefendigil F, Öztop H. Influence of inclination angle of magnetic filed on mixed convection of nanofluid flow over a backward facing step and entropy generation. Adv. Powder Tech. 2015;26:1663–75.

[36] Iqbal Z, Maraj EN, Azhar E, Mehmood Z. A novel development of hybrid $(MoS_2 - SiO_2/H_2O)$ nanofluidic curvilinear transport and consequences for effectiveness of shape factors. J. Taiwan Inst. Chem. Eng. 2017;81:150–8.

[37] Awad FG, Sibanda P, Motsa SS, Makinde OD. Convection from an inverted cone in a porous medium with cross-diffusion effects. Comp. Math. Appl. 2011;61:1431–41.